JVSTA Journal of Vacuum Science & Technology A

Defects in nonpolar (13 4 ¯ 0) ZnO epitaxial film grown on (114) LaAlO3 substrate

Tzu-Chun Yen, Wei-Lin Wang, Chun-Yen Peng, Jr-Sheng Tian, Yen-Teng Ho, and Li Chang

Citation: Journal of Vacuum Science & Technology A **32**, 02B103 (2014); doi: 10.1116/1.4830275
View online: http://dx.doi.org/10.1116/1.4830275
View Table of Contents: http://scitation.aip.org/content/avs/journal/jvsta/32/2?ver=pdfcov
Published by the AVS: Science & Technology of Materials, Interfaces, and Processing

Defects in nonpolar (13$\bar{4}$0) ZnO epitaxial film grown on (114) $LaAlO_3$ substrate

Tzu-Chun Yen,[a] Wei-Lin Wang, Chun-Yen Peng, Jr-Sheng Tian, Yen-Teng Ho, and Li Chang
Department of Materials Science and Engineering, National Chiao Tung University, Hsinchu 30010, Taiwan

(Received 15 August 2013; accepted 18 October 2013; published 20 November 2013)

The defects in (13$\bar{4}$0)ZnO epitaxial film grown on (114)$LaAlO_3$ (LAO) have been systematically investigated by using transmission electron microscopy. At the ZnO/LAO interface, the Burgers vectors of misfit dislocations are identified to be 1/3[$\bar{1}$2$\bar{1}$0] and 1/2[0001]. Threading dislocations with the Burgers vectors of 1/3⟨11$\bar{2}$0⟩ and ⟨0001⟩ are distributed on the basal plane. In (13$\bar{4}$0)ZnO film, the predominant planar defects are basal stacking faults (BSFs) with 1/6⟨20$\bar{2}$3⟩ displacement vectors. The densities of dislocations and BSFs are about $3.8 \times 10^{10}\,cm^{-2}$ and $3.1 \times 10^{5}\,cm^{-1}$, respectively. © *2014 American Vacuum Society*. [http://dx.doi.org/10.1116/1.4830275]

I. INTRODUCTION

As a wide direct band gap semiconductor, wurtzite ZnO has been considered as a potential candidate for optoelectronic applications due to its high exciton binding energy (~60 meV), which allows high ultraviolet-lasing efficiency.[1] However, conventional [0001]-oriented ZnO-based quantum wells suffer from discontinuous polarization known as quantum confined Stark effect (QCSE). The effect causes spatial separation of electrons and holes, and therefore emission efficiency droops.[2–4] To avoid QCSE, it is desirable to grow ZnO in nonpolar orientations, such as *a*-plane (11$\bar{2}$0) and *m*-plane (10$\bar{1}$0).[5,6] To obtain nonpolar ZnO films, many studies have proposed alternative substrates for the growth of nonpolar ZnO.[7–9]

Recently, we have also demonstrated the epitaxial growth of nonpolar (13$\bar{4}$0) ZnO epitaxial films on (114) $LaAlO_3$ (LAO) substrate.[10] The ZnO thin films have the epitaxial relationship of $[0001]_{ZnO}//[\bar{1}10]_{LAO}$ with the lattice mismatch of 2.9% and 3% along $[\bar{1}10]_{LAO}$ and $[22\bar{1}]_{LAO}$, respectively. Since crystalline defects in *a*- and *m*-plane ZnO profoundly affect electronic and optical properties, it will be of great interest to understand their characteristics and distribution in (13$\bar{4}$0)ZnO.

II. EXPERIMENT

Growth of (13$\bar{4}$0)ZnO on (114)LAO substrate was carried out by pulsed laser deposition at 750 °C in oxygen ambient of 20 mTorr. The detailed process has been described elsewhere.[10] Defect observations in (13$\bar{4}$0)ZnO film were performed in Philips Tecnai 20 and JEOL JEM 2100F transmission electron microscopes (TEM) operated at 200 kV. Two cross-sectional TEM (XTEM) specimens along [$\bar{1}$10]LAO and [22$\bar{1}$]LAO and one plan-view TEM (PV-TEM) specimen near along [$\bar{1}\bar{1}$20]ZnO (~16° away from [13$\bar{4}$0]) were prepared by mechanical grinding and Ar^+ ion milling.

III. RESULTS AND DISCUSSION

Figures 1(a) and 1(b) are the selected area diffraction (SAD) patterns taken from the interfacial region of (13$\bar{4}$0) ZnO on (114) LAO substrates in zone axes of [$\bar{1}$10]LAO and [22$\bar{1}$]LAO, respectively. The identified SAD patterns clearly indicate that ZnO grown on (114) LAO forms a single crystalline thin film with the in-plane epitaxial relationship of [0001]ZnO//[$\bar{1}$10]LAO. In addition, it is found that the (13$\bar{4}$0)ZnO plane has a small inclination (~0.5°) to (114)LAO plane according to the measurement in the SAD pattern in Fig. 1(a). The observation is consistent with the previous report from the investigation of x-ray diffraction.[10]

For the hetero-epitaxial structure, the misfit dislocations (MDs) commonly appear at the heterointerface for the relaxation of mismatch-induced strain. For the observations of MDs, the high resolution XTEM images of (13$\bar{4}$0)ZnO/(114)LAO interface taken under two perpendicular directions, corresponding to Figs. 1(a) and 1(b), are shown in Figs. 2(a) and 2(b). Figure 2(a) presents the image of the ZnO/LAO interface along zone axis [1$\bar{1}$0]LAO, where two MDs can be identified with the closure failure of Burgers circuits, with white dots indicating the start and end points. The Burgers vectors of the MDs are b = 1/3[$\bar{1}$2$\bar{1}$0]. Owing to the small lattice mismatch (~3%) along [22$\bar{1}$]LAO, only two MDs are found in the observed regions. As measured, the distance between two MDs is 11.1 nm along [22$\bar{1}$]LAO slightly larger than the calculated value of 9.8 nm. Figure 2(b) is the image of the ZnO/LAO interface (marked with dashed line) taken along zone axis of [22$\bar{1}$]LAO. As known from the observation in Figs. 1(a) and 1(b), the ZnO film is close to zone axis [25$\bar{7}$0] in Fig. 2(b). Three extra half-planes, as marked with circles in Fig. 2(b), are observed, from which the Burgers vector for the MDs is 1/2[0001] which is certainly parallel to the interface. In Fig. 2(b), the measured distances between adjacent MDs is 9.4 and 7.0 nm (average ~8.2 nm) along the [0001]ZnO direction close to the calculated value of 9.0 nm. The uneven distance among MDs might be related to the formation of stacking faults or nonuniformation strain relaxation.

For the further investigation of the defects in (13$\bar{4}$0)ZnO film on (114)LAO, XTEM, and PV-TEM analyses are

[a]Electronic mail: yen198300@gmail.com

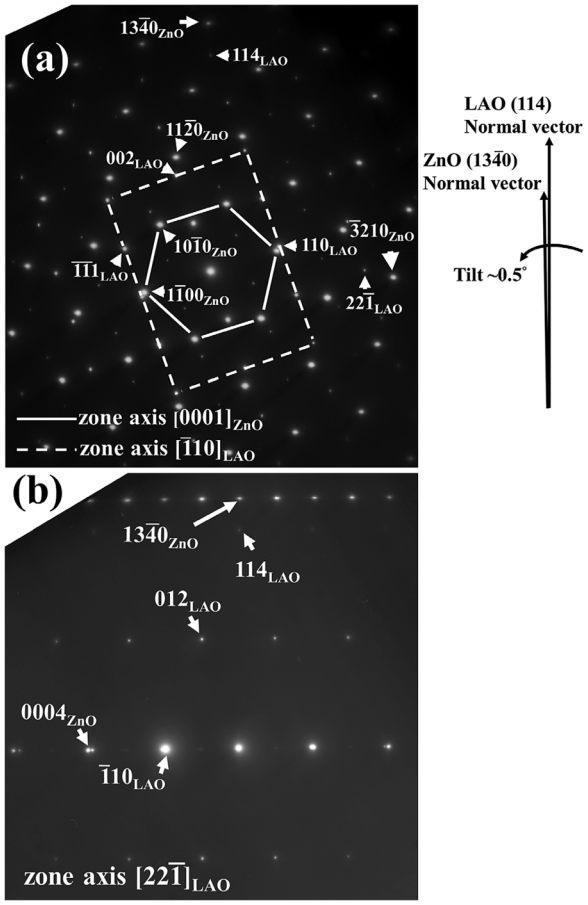

FIG. 1. TEM SAD patterns taken near the interfacial region of ZnO/LAO in zone axes of (a) $[\bar{1}10]_{LAO}$ and (b) $[22\bar{1}]_{LAO}$, respectively.

carried out under two-beam conditions using $g \cdot R = 0$ invisibility criterion, where g is a chosen diffraction vector and R is the Burgers vector (b) or displacement vector of stacking faults. It has been known that in nonpolar ZnO the predominant line defects are threading dislocations (TDs) with $b = 1/3\langle 11\bar{2}0\rangle$, $1/3\langle 11\bar{2}3\rangle$, and $\langle 0001\rangle$ and the predominant planar defects are basal stacking faults (BSFs) with the displacement vectors of $1/6\langle 20\bar{2}3\rangle$. In Fig. 3(a), the bright field XTEM (BF-XTEM) image of (13$\bar{4}$0) ZnO film taken near zone axis [0001]ZnO with $g = \bar{1}\bar{1}20$ mainly shows TDs with $b = 1/3\langle 11\bar{2}0\rangle$ and $1/3\langle 11\bar{2}3\rangle$. In the observation along [0001]ZnO, the TDs in wigglelike contrast are identified to be mixed or 60°-type dislocations similar to those in a-plane films. Figure 3(b) obtained from the other XTEM specimen is the BF-XTEM image taken near zone axis $[22\bar{1}]$LAO, where ZnO $g = 0002$ is nearly satisfied. In Fig. 3(b), the TDs with $b = \langle 0001\rangle$ and $1/3\langle 11\bar{2}3\rangle$ extend straight upward to the surface from the interface. Figure 3(c) is the BF-XTEM image formed by tilting the specimen to be near zone axis $[\bar{2}110]$ZnO with $g = 01\bar{1}0$, showing that BSFs and TDs with $b = 1/3\langle 11\bar{2}0\rangle$ are in contrast. After further tilting the specimen 30° angle from zone axis $[\bar{2}110]$ZnO to near zone axis $[\bar{1}100]$ZnO with $g = 11\bar{2}0$, the BF-XTEM image obtained is shown in Fig. 3(d) which reveals TDs with $b = 1/3\langle 11\bar{2}0\rangle$. From Figs. 3(c) and 3(d), the TDs and BSFs show the behavior of extending vertically toward the surface. By comparing the TD behavior observed from different directions [Figs. 3(a)–3(d)], it can be concluded that all TDs lie on the c-planes in the (13$\bar{4}$0)ZnO thin film.

In order to realize the distribution of TDs and BSFs, PV-TEM images taken near zone axis $[\bar{1}\bar{1}20]$ZnO with $g = \bar{1}100$ and $g = 0002$ diffraction conditions are, respectively, presented in Figs. 4(a) and 4(b). As shown in Fig. 4(a), BSFs marked by white arrows align parallel to the basal plane and the density of the BSFs is about $3.1 \times 105\ \mathrm{cm}^{-1}$. In Fig. 4(b),

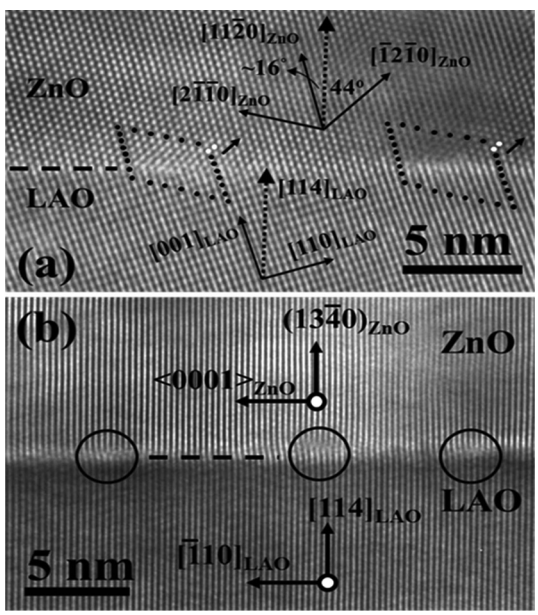

FIG. 2. HR-XTEM images of (13$\bar{4}$0)ZnO/(114)LAO interface taken under zone axes of (a) $[\bar{1}10]_{LAO}$ and (b) $[22\bar{1}]_{LAO}$.

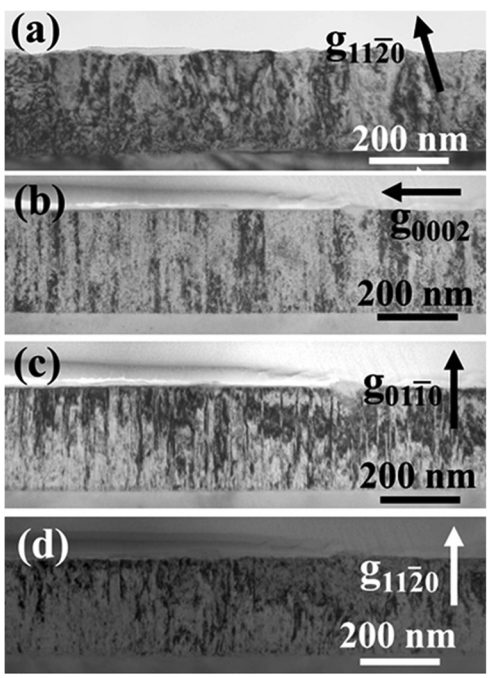

FIG. 3. BF-XTEM image taken near zone axis $[0001]_{ZnO}$ with $g = 11\bar{2}0$. BF-XTEM images taken near zone axis $[\bar{2}110]_{ZnO}$ with (b) $\mathbf{g} = 0002$ and (c) $\mathbf{g} = 01\bar{1}0$. (d) BF-XTEM image taken near zone axis $[\bar{1}100]_{ZnO}$ with $\mathbf{g} = 11\bar{2}0$.

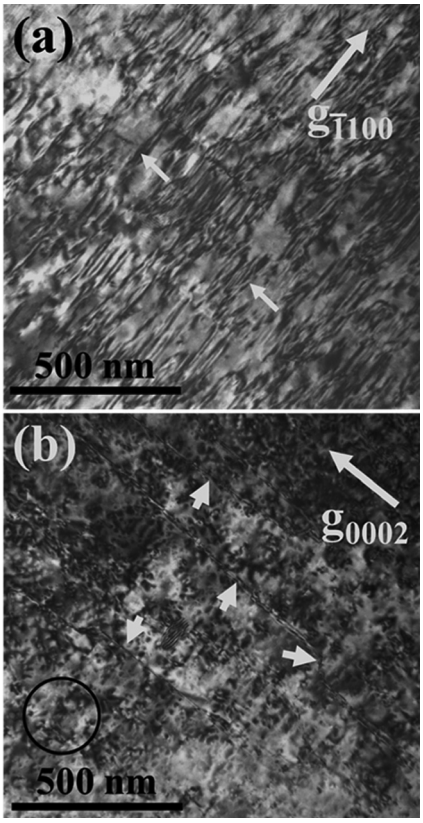

FIG. 4. PV-TEM images taken near zone axis $[\bar{1}\bar{1}20]_{ZnO}$ with (a) $\mathbf{g} = \bar{1}100$ and (b) $\mathbf{g} = 0002$.

the image reveals the end-on contrast of dislocations as circled with black solid line and line contrast of prismatic mismatch boundaries as white-arrowed. In the PV-TEM image, the dislocations with end-on contrast include TDs and BSF-bounded partial dislocations. Thus, the estimated dislocation density is around $3.8 \times 10^{10}\,\mathrm{cm}^{-2}$ in the (13$\bar{4}$0)ZnO film.

IV. CONCLUSIONS

TEM observations present the line and planar defects in nonpolar (13$\bar{4}$0)ZnO epitaxial film grown on (114)LAO substrate. At the ZnO/LAO interface, the Burgers vectors of MDs are 1/3[$\bar{1}2\bar{1}0$] and 1/2[0001] along [22$\bar{1}$]LAO and [1$\bar{1}$0]LAO, respectively. Most of TDs have Burgers vectors of 1/3$\langle 11\bar{2}0\rangle$ and lie on the basal plane of ZnO. The density of total dislocation density is about $3.8 \times 10^{10}\,\mathrm{cm}^{-2}$, and the density of the BSFs is around $3.1 \times 10^{5}\,\mathrm{cm}^{-1}$.

ACKNOWLEDGMENT

This research was partially supported by the National Science Council of Taiwan, R.O.C., under Contract No. NSC 101-2221-E-009-049-MY3.

[1]M. H. Huang, S. Mao, H. Feick, H. Yan, Y. Wu, H. Kind, E. Weber, R. Russo, and P. Yang, Science **292**, 1897 (2001).
[2]J.-M. Chauveau, M. Laügt, P. Venneguès, M. Teisseire, B. Lo, C. Deparis, C. Morhain, and B. Vinter, Semicond. Sci. Technol. **23**, 035005 (2008).
[3]H. Matsui, N. Hasuike, H. Harima, and H. Tabata, J. Appl. Phys. **104**, 094309 (2008).
[4]J -M. Chauveau, M. Teisseire, H. Kim-Chauveau, C. Deparis, C. Morhain, and B. Vinter, Appl. Phys. Lett. **97**, 081903 (2010).
[5]Y. T. Ho, W. L. Wang, C. Y. Peng, M. H. Liang, J. S. Tian, C. W. Lin, and L. Chang, Appl. Phys. Lett. **93**, 121911 (2008).
[6]Y. T. Ho, W. L. Wang, C. Y. Peng, W. C. Chen, M. H. Liang, J. S. Tian, and L. Chang, Phys. Status Solidi RRL **3**, 109 (2009).
[7]A. Ohtomo and A. Tsukazaki, Semicond. Sci. Technol. **20**, S1 (2005).
[8]E. Bellingeri, D. Marré, I. Pallecchi, L. Pellegrino, G. Canu, and A. S. Siri, Thin Solid Films **486**, 186 (2005).
[9]T. Nakamura, H. Minoura, and H. Muto, Thin Solid Films **405**, 109 (2002).
[10]Y. T. Ho, W. L. Wang, C. Y. Peng, J. S. Tian, Y. S. Shih, T. C. Yen, and L. Chang, Phys. Status Solidi RRL **6**, 114 (2012).